Desalination and Water Treatment
www.deswater.com
doi: 10.5004/dwt.2023.29639

296 (2023) 137–146
June

Effective removal of anionic dye from aqueous solutions using modified carbonate material: performance and mechanism

Samira Ziane[a,*], Fatiha Bessaha[a], Nouria Mahrez[a], Fatima Boucif[a], Kheira Marouf-Khelifa[a], Ali Çoruh[b], Amine Khelifa[a]

[a]*Laboratory of Structure, Elaboration and Applications of Molecular Materials (S.E.A.2M.), Department of Process Engineering, University of Mostaganem, B.P. 981, R.P., Mostaganem 27000, Algeria, Tel.: +213 45 20 45 85; Fax: +213 45 21 10 18; emails: samirazianedz@gmail.com (S. Ziane), fatiha_bessaha@yahoo.fr (F. Bessaha), nour411@gmail.com (N. Mahrez), boucif78@yahoo.fr (F. Boucif), kheira_marouf@yahoo.fr (K. Marouf-Khelifa), aminekhelifadz@yahoo.fr (A. Khelifa)*
[b]*Department of Physics, Sakarya University, 54147-Kampus, Sakarya, Turkey, email: coruh@sakarya.edu.tr*

Received 19 April 2022; Accepted 11 May 2023

ABSTRACT

In this study, a carbonate material (CM) and its form heated to 900°C (CM900) were used to remove Congo red (CR) from aqueous solutions. The objective was to combine the results of the characterization of the modified material, CR adsorption and spectroscopic study to propose a coherent mechanism of the CR-CM900 interaction. A bibliographical study on the adsorption of dyes by carbonates and their interactions revealed the scarcity of published works. This study will compensate somewhat for the lack of results in this field. Carbonate materials are abundant, low-cost and available in different countries around the world. The materials were characterized by X-ray diffraction and scanning electron microscopy. A solid/solution concentration of 1 $g \cdot L^{-1}$, pH of 6.9, equilibrium time of 2 h and temperature of 40°C, were found to be the optimum conditions for a maximum amount of CR adsorbed by CM900 of 288.2 against 32.7 $mg \cdot g^{-1}$ for CM. A full decarbonation of CM900 results in MgO and CaO, releases CO_2 from the structure, and leads to a more porous structure. The pseudo-first-order model adequately described the kinetic data. The experimental isotherms were suitably fitted by the Redlich–Peterson model with determination coefficient and average relative error values ≥0.97% and <10.0%, respectively. Thermodynamic parameters suggested a spontaneous and endothermic process. Methanol easily desorbed the CR adsorbed by CM900 which maintained its adsorption capacity during three adsorption–desorption cycles. Fourier-transform infrared spectroscopy investigation before and after the dye adsorption showed that the CR-CM900 interaction involves a mechanism of outer-sphere complexation between the amine groups and the hydroxylated magnesium oxides. Understanding the interactions between dyes and carbonate materials is an important approach to develop the use of these materials in wastewater treatment.

Keywords: Carbonate material; Removal; Congo red; Fourier-transform infrared spectroscopy; Mechanism

1. Introduction

Industrial and technological progress on a global scale has introduced different organic and inorganic contaminants into the water resources, which include organic dyes, pharmaceuticals, personal care products, heavy metals, and toxic chemicals [1–4]. Their presence in industrial effluents or drinking water constitutes a public health problem

* Corresponding author.

1944-3994/1944-3986 © 2023 Desalination Publications. All rights reserved.

because of their absorption and subsequent accumulation in the human body.

Synthetic dyes are widely used in textile industries. The annual production of synthetic dyes is approximately one million tons. In industrial effluents, about 15% of the azo dyes are discharged. Since they are recalcitrant organic molecules, immune to aerobic digestion, stable to light, heat and oxidizing agents, their existence in wastewater causes health and aquatic problems [5]. Among the azo dyes, Congo red (CR) was chosen in this study, because it is extensively used. Its ubiquitous presence in wastewaters has adverse effects on aquatic life and health, due to its biorefractory, carcinogenic, and persistent characteristics [6]. Several techniques have been reported to remove Congo red from wastewater: photocatalytic degradation, biological and electrochemical treatments, chemical precipitation, ion-exchange, nanofiltration, and adsorption [7–11]. Most of these processes have limitations due to complex operations, poor cost effectiveness, removal issues, and sometimes low removal performance.

Adsorption has developed as a green and efficient approach based on cost, performance and ecology. It has numerous benefits, including easy design and use under mild conditions and at wide pH range, efficiency at low pollutant concentrations, selectivity, and reusability [12]. Adsorption technology is also well adapted for the treatment of wastewater released from textile industries [13]. Various inexpensive adsorbents were used to remove Congo red from wastewater, such as chir pine sawdust, bentonite, calcium alginate, and cross-linked chitosan [14–17].

A carbonate material (CM) is an important industrial mineral. It is considered as a salt combining a carbonate ion (CO_3^{2-}) with one or more cations. There are different types of carbonate materials such as aragonite and calcite ($CaCO_3$), magnesite ($MgCO_3$) and dolomite ($CaMg(CO_3)_2$). The latter is an abundant natural mineral of stoichiometric formula $CaMg(CO_3)_2$, consisting of an alternation of Ca^{2+} and Mg^{2+} planes. A review of the literature revealed that dolomite has been used as ceramic and catalyst [18–21], but very few studies have been published on this carbonate material as an adsorbent, mainly because of its poor properties. After an appropriate modification and characterization, the material was used in the adsorption of Congo red from aqueous solutions. The objectives of this study were to enhance the adsorptive properties of this carbonate material and to combine the results of its characterization, CR adsorption and spectroscopic study to propose a coherent mechanism of the CR-carbonate material interaction. Understanding the interactions between dyes and carbonate materials is an important approach to develop the use of these materials in wastewater treatment.

Dolomite as a carbonate material (CM) was processed at 900°C (CM900) and analyzed by X-ray diffraction (XRD), scanning electron microscopy (SEM) and Fourier-transform infrared spectroscopy (FTIR) before and after CR adsorption. The adsorption of CR was performed through the parameters contact time, equilibrium data and temperature. Desorption was studied using five eluents. Five regeneration cycles (adsorption/desorption) were carried out for CM900, the best adsorbent. The FTIR study was also conducted to understand the mechanism of the CR-CM900 interaction.

2. Materials and methods

2.1. Materials

The natural carbonate material used in this research comes from the western region of Algeria. Its chemical composition is: MgO: 21.05%, CaO: 31.18%, Fe_2O_3: 0.02%, Al_2O_3: 0.002%, SiO_2: 0.01%, MnO_2: 0.0015% and Cr_2O_3: 0.01%. The crude material was calcined for 2 h at 900°C, which led to the formation of mixed CaO and MgO oxides [22]. The crude material and its calcined form were designated CM and CM900, respectively.

2.2. Characterization

X-ray powder diffraction patterns were obtained using a Philips PW 1830 diffractometer (Netherlands) with CoKa radiation (λ = 0.1789 nm). XRD data were collected over a 2θ range of 5°–90° with a step width of 0.03°. This range was chosen to identify the main and secondary peaks. Each sample required 25 min of analysis. The crystallite size and morphology of the samples were determined by scanning electronic microscopy (JEOL, JSM-6360, Japan). Infrared (IR) spectra were recorded on a Shimadzu Prestige 21 spectrophotometer (Japan) using a KBr pellet technique containing 0.5% sample.

2.3. Procedure for adsorption and desorption

Dye used is Congo red (CR), an anionic dye belonging to the azo class. A stock solution of 1,000 mg·L^{-1} of CR (chemical formula: $C_{32}H_{22}O_6N_6S_6Na_2$, molecular weight: 696.7 g·mol^{-1}, supplied by Merck) was prepared by dissolving a suitable amount of dye in distilled water. The working solutions were prepared by diluting a certain volume of the stock solution in a volume corresponding to the new concentration to be prepared. 20 mg (m) of each sample (CM or CM900) was mixed with 20 mL (V) of aqueous solution of the different prepared concentrations and at a pH of 6.9. The suspension was then centrifuged and the supernatant was assayed by visible spectrophotometry at 498 nm using a Shimadzu 1240 UV/Vis instrument (Japan). Adsorbed amounts, Q_{exp} (mg·g^{-1}), were calculated using the equation $Q_{exp} = (C_0 - C_e)\ V/m$, where $V/m = 1$ and C_0 and C_e are initial and equilibrium concentrations (mg·L^{-1}), respectively.

Desorption experiments were performed by mixing 50 mg of CR-loaded CM900 with 50 mL of eluent. After stirring for 120 min, CM900 was recovered and the amount of CR released into the eluent was determined spectrophotometrically. Five eluents were used to desorb CR from CM900. The best eluent (methanol) was used for CM900 regeneration. Five successive adsorption–desorption cycles were conducted and after each cycle, the recovered adsorbent was dried at 90°C. All experiments were performed in triplicate, and only the average results are reported in this paper. The conditions used are listed in Table 1.

2.4. Theoretical approach

2.4.1. Kinetic modeling

The adsorption kinetics may be described by a pseudo-first-order [Eq. (1)], a pseudo-second-order [Eq. (2)],

intraparticle diffusion [Eq. (4)] and Elovich reaction [Eq. (5)], respectively [23–26].

$$\log\left(Q_s - Q_t\right) = \log Q_s - \frac{K_1 t}{2.303} \quad (1)$$

where Q_e: quantity adsorbed at equilibrium (mg·g^{-1}); Q_t: quantity adsorbed at time t (mg·g^{-1}); K_1: pseudo-first-order velocity constant (min^{-1}); t: contact time (min).

$$\frac{t}{Q_t} = \frac{1}{K_2 \cdot Q_e^2} + \frac{t}{Q_e} \quad (2)$$

where K_2 is the pseudo-second-order velocity constant (g·mg^{-1}·min^{-1}).

The initial adsorption rate, h, at $t \to 0$ is defined as:

$$h = K_2 \cdot Q_e^2 \quad (3)$$

where h, Q_e and K_2 are obtained from the slope and ordinate at the origin of the linear plot of t/Q_t vs. t.

$$Q_t = k_{\text{id}} \cdot t^{\frac{1}{2}} + 1 \quad (4)$$

where k_{id} is the intraparticle diffusion rate constant (mg·g^{-1}·min$^{-1/2}$) and C is a constant.

The values k_{id} and C are calculated from the angle and the interception, respectively, of the plot of Q_t vs. $t^{1/2}$.

$$Q_t = \frac{1}{\beta}\ln\left(\alpha \cdot \beta\right) + \frac{1}{\beta}\ln t \quad (5)$$

where α: Initial adsorption rate (mg·g^{-1}·min^{-1}); β: is the desorption constant (g·mg^{-1}). The coefficients α and β are calculated from the plot Q_t vs. ln$t$.

2.4.2. Modeling adsorption isotherms

The Langmuir, Freundlich and Redlich–Peterson (RP) models were used to fit the experimental isotherms. Their equations are given in Table 2.

A model is validated on the basis of the parameters coefficient of determination, R^2, and average relative error, E%. The latter is given by:

$$E\% = \frac{100}{n}\sum_{i=1}^{n}\left|\frac{Q_{\exp_i} - Q_{\text{cal}_i}}{Q_{\exp_i}}\right| \quad (9)$$

where $Q_{\exp_i}$: quantity adsorbed at equilibrium (mg·g^{-1}); Q_{cal_i}: calculated adsorbed quantity (mg·g^{-1}); n: number of experimental data.

2.4.3. Thermodynamics study

The thermodynamic parameters of the CR adsorption were established using the following relation:

$$\ln K_d = \left(\frac{-\Delta H^\circ}{R \cdot T}\right) + \left(\frac{\Delta S^\circ}{R}\right) \quad (10)$$

where ΔH°: enthalpy (kJ·mol^{-1}); ΔS°: variation of entropy (J·mol^{-1}·K^{-1}); R: gas constant (J·mol^{-1}·K^{-1}); K_d: coefficient of distribution; T: absolute temperature (K).

Table 1
Experimental conditions during the adsorption of Congo red by CM and CM900

Contact time	1, 3, 5, 10, 20, 40, 60, 120, and 240 min; C_{initial} = 80 mg·L^{-1}, [solid]/[solution]: 1 g·L^{-1}, T = 25 and 40°C, pH: 6.9
Concentration	20, 40, 60, 80, 100, 150, 200, 300, and 400 mg·L^{-1}; contact time: 120 min; pH: 6.9
Temperature	25°C and 40°C. [solid]/[solution]: 1 g·L^{-1}; time of contact: 120 min; pH: 6.9
Desorption	Solvents: water (H_2O); methanol (CH_3OH); ethanol (C_2H_6O); acetone (C_3H_6O); 50% water + 50% methanol; adsorbent: CM900
Regeneration	Eluant: methanol; five adsorption/desorption cycles

Table 2
Isotherm equations applied to fit the experimental data

Adsorption models	Equations	Parameters
Langmuir [27]	$Q_e = Q_m \frac{K_L C_e}{1 + K_L C_e}$ (6)	Q_e: equilibrium amount removed from solution (mg·g^{-1}) C_e: equilibrium concentration (mg·L^{-1}) Q_m: maximum amount per unit weight of adsorbent for complete monolayer coverage (mg·g^{-1}) K_L: constant related to the affinity of binding sites (L·mg^{-1})
Freundlich [28]	$Q_e = K_F C_e^{1/n}$ (7)	K_F: constant taken as an indicator of adsorption capacity (L·g^{-1}) $1/n$: constant indicative of the adsorption intensity
Redlich–Peterson [29]	$Q_e = \frac{K_R C_e}{1 + a_R C_e^{\beta}}$ (8)	Q_e: amount adsorbed at equilibrium (mg·g^{-1}) C_e: equilibrium solution concentration (mg·L^{-1}) K_{RP}: equilibrium constant (L·mg^{-1}) β: heterogeneity factor that depends on surface properties of the adsorbent a_{RP}: maximum amount adsorbed (mg·g^{-1})

$$K_d = \frac{Q_e}{C_e} \tag{11}$$

The variation of entropy values were evaluated by:

$$\Delta G° = \Delta H° - T\Delta S° \tag{12}$$

3. Results and discussion

3.1. Characterization

The powder XRD patterns of CM and CM900 are presented in Fig. 1. The diffractogram of CM displays a sharp peak that could be attributed to the $CaCO_3 \cdot MgCO_3$ phase. Carbonate material treated at 900°C, CM900, decomposes into magnesium oxide and calcium oxide. CM900 thus undergoes a total decarbonation with formation of CaO and MgO.

SEM images of CM and CM900 are depicted in Fig. 2. The SEM analysis of CM indicates the presence of cleavages and shows an apparent preferential orientation of crystals along *c*-axis.

After thermal modification, significant changes of the surface topography of CM900 happen. The corresponding micrograph highlights the newly created pores and slots. The structure appears to be less compact than that of CM. These features could be explained by the decarbonation of $CaCO_3 \cdot MgCO_3$. The released CO_2 leads to a more porous structure [22,30].

3.2. Congo red adsorption

3.2.1. Kinetics

All experiments were conducted at a pH of 6.9 because CR adsorption is maximal (figure not shown). The kinetic curves of CR adsorption are given in Fig. 3. Adsorption rate is rapid in the first 40 min and then gradually decreases and reaches equilibrium at about 2 h. Further increase in contact time did not change significantly CR removal. Fast

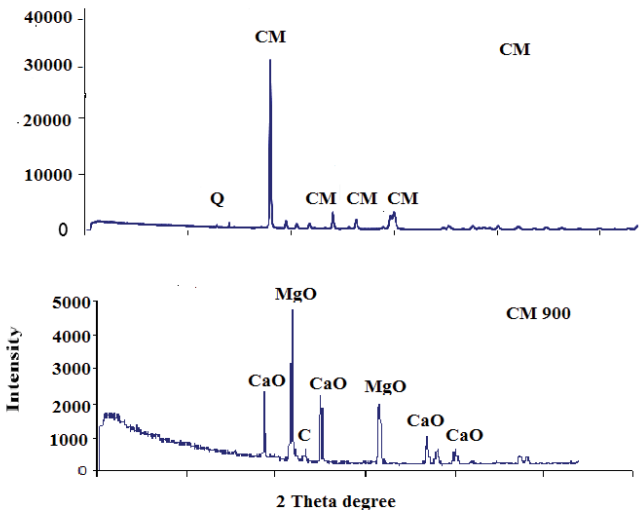

Fig. 1. X-ray diffraction patterns of carbonate material and its form heated to 900°C (CM900).

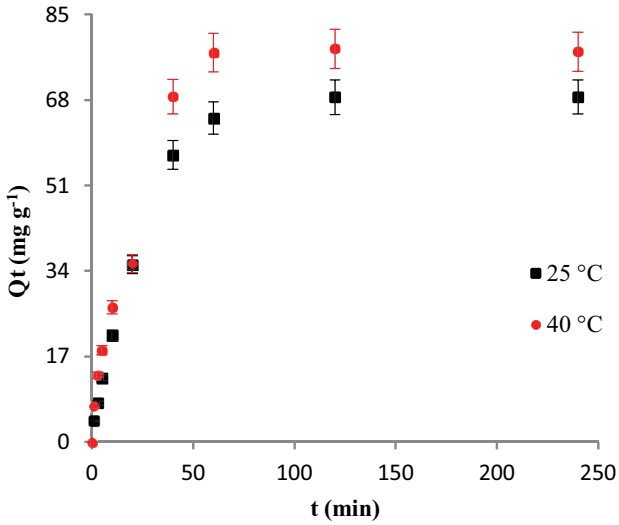

Fig. 3. Effect of contact time on the adsorption of Congo red by CM900 at 25°C and 40°C.

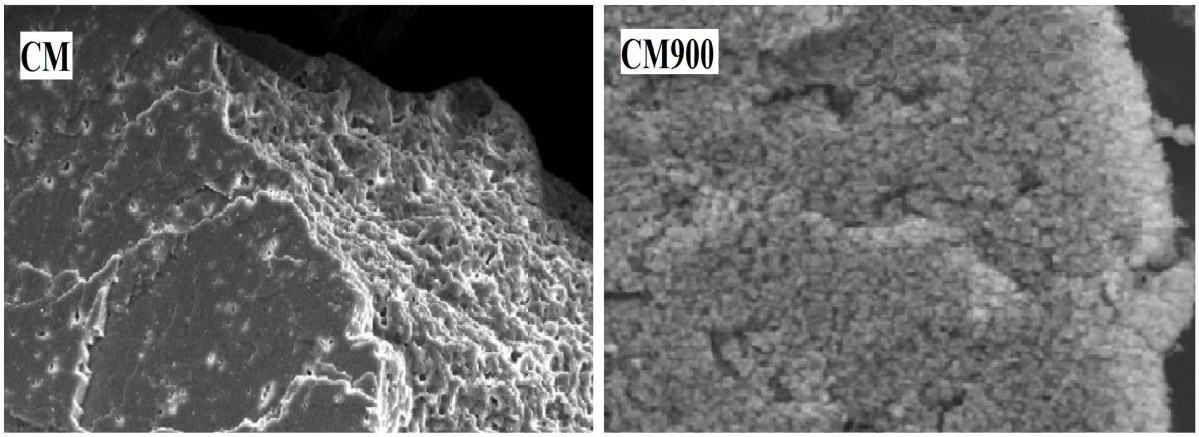

Fig. 2. Scanning electron microscopy images of carbonate material and its form heated to 900°C (CM900).

adsorption at the initial contact time is due to the availability of adsorption sites on the material surface. 2 h seems to be a sufficient time to reach equilibrium for different pollutant/material systems, such as chloramphenicol/modified halloysite [31], RB5/dolomite [32], and heavy metals/biosorbent [33].

Several models were applied to fit the experimental kinetic data. The fit of the experimental data with the pseudo-first-order model is appropriate for CM and CM900. The Q_e(exp) and Q_e(cal) values are in close agreement, with a deviation <5% and a R^2 value ≥ 0.98 for CM900 (Table 3). The validity of the pseudo-first-order model indicates that adsorption mainly involves physical interactions, based on a diffusion process for which the occupancy rate of the adsorption sites is proportional to the number of unoccupied sites [34,35]. The pseudo-second-order model led to a significant divergence between experimental and theoretical values of the amount adsorbed at equilibrium, which shows the inadequacy of this model. For illustration, the experimental and theoretical amounts adsorbed by CM at 40°C were 28.3 and 61.4 mg·g^{-1}, respectively. When a batch mode adsorption is used, the possibility of the intraparticle pore diffusion of adsorbate is always present. High R^2 values (0.988–0.998) were obtained (Table 3), corresponding to intraparticle diffusion. The intraparticle diffusion rate constant, k_{id}, increased with temperature, which indicates an enhancement of the pore diffusion into CM and CM900 particles. The l value gives an insight of the boundary layer thickness. The l value of CM900 is 18 times larger than that of CM. Heat treatment disturbs the interfacial properties of carbonate material, so that the effect of the boundary layer plays a major role in Congo red adsorption. The boundary layer thickness also significantly influenced the adsorption of catechol by a dolomite treated at 800°C [36]. The Elovich model is one of the most used to describe chemisorption on highly heterogeneous adsorbents. Its parameters were calculated from the plot of Q_t vs. ln$t$ [Eq. (5)] [26]. For a majority of samples, the R^2 values are close to 0.9, which confirms the non-validity of this model.

3.2.2. Isotherms and affinity

The adsorption isotherms of CR at 25 and 40°C by CM900 are given in Fig. 4. They show typical Langmuir-shaped isotherms. The amount of CR adsorbed increases with increasing initial concentration until equilibrium is reached. The first part of the curve reveals that CR has a strong affinity with the material surface. The amount adsorbed increases with increasing temperature, regardless of the material examined. CM900 adsorbs 261.36 and 288.18 mg·g^{-1} at 25

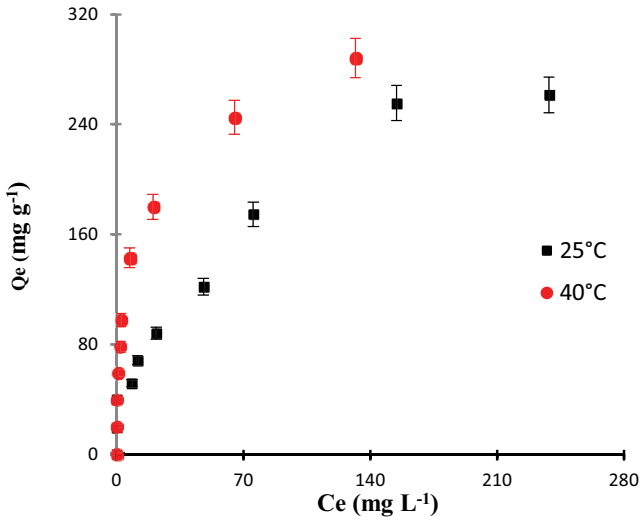

Fig. 4. Isotherms of the adsorption of Congo red on CM900 at 25°C and 40°C.

Table 3
Kinetic parameters of Congo red adsorption on carbonate materials CM and CM900

Models	Parameters	Adsorbents			
		CM		CM900	
		25°C	40°C	25°C	40°C
Pseudo-first-order	Q_e(exp) (mg·g^{-1})	15.80	28.322	68.59	77.60
	Q_e(cal) (mg·g^{-1})	18.66	38.21	69.69	79.89
	K_1 (min^{-1})	0.0091	0.0069	0.039	0.041
	R^2	0.972	0.927	0.997	0.977
Pseudo-second-order	Q_e(cal)	27.54	61.43	80.76	91.39
	K_2 (g·mg^{-1}·min^{-1})	0.00024	0.00007	0.0006	0.0005
	h (mg·g^{-1}·min^{-1})	0.182	0.264	3.913	4.176
	R^2	0.967	0.921	0.980	0.956
Intraparticle diffusion	k_{id} (mg·g^{-1}·min$^{-1/2}$)	0.089	0.126	1.25	1.42
	l (mg·g^{-1})	0.757	0.582	8.13	10.70
	R^2	0.994	0.998	0.992	0.988
Elovich	α (mg·g^{-1}·min^{-1})	0.00024	0.00007	5.80	8.07
	β (g·mg^{-1})	27.54	61.44	0.055	0.051
	R^2	0.966	0.921	0.938	0.915

and 40°C, respectively, and for an initial concentration of 400 mg·L^{-1}. An increase in temperature intensifies diffusion which leads to an increase in adsorbed amount, and generally indicating that the interaction mechanism of adsorbate/adsorbent systems would be an activated process [37].

The affinity of CM900 for Congo red is much higher than that of CM, the uptake being 288.18 and 32.73 mg·g^{-1} at 40°C, respectively (Fig. 5). A dolomite heated to 900°C was also found to be a better adsorbent than untreated dolomite for Orange I adsorption [38]. The significantly higher adsorption of CM900 compared to CM may be explained from its crystallographic properties. A full decarbonation of CM900 results in MgO and CaO, releases CO_2 from the structure, and leads to a more porous structure. In contrast, the lower adsorption potential of the starting material, CM, could be due to the presence of a $CaCO_3$·$MgCO_3$ phase without decarbonation, dense, for which there is no mass loss [32]. These explanations are corroborated by the XRD and SEM analyses.

3.2.3. Comparison of Congo red onto CM900 adsorption with other adsorbent materials

The adsorption capacity of CR by CM900 was compared to that of various adsorbents (Table 4). As shown, the Q_{max} of CM900 (288.2 mg·g^{-1}) is significantly higher than that of materials such as sawdust, activated carbon, bentonite, calcium alginate, and $Ni(OH)_2$. This material appears to be very effective in removing Congo red.

3.2.4. Modelling of experimental isotherms

The fitting of experimental isotherms by theoretical isotherms is crucial for the simulation of adsorption processes and the prediction of adsorbed amounts for experimentally unexploited contaminant concentrations. The validity of the model is represented by the average relative error (E%) and coefficient of determination (R^2). The Freundlich, Langmuir and Redlich–Peterson models used in this study and their parameters are listed in Table 2. The results of the models used are described in Table 5.

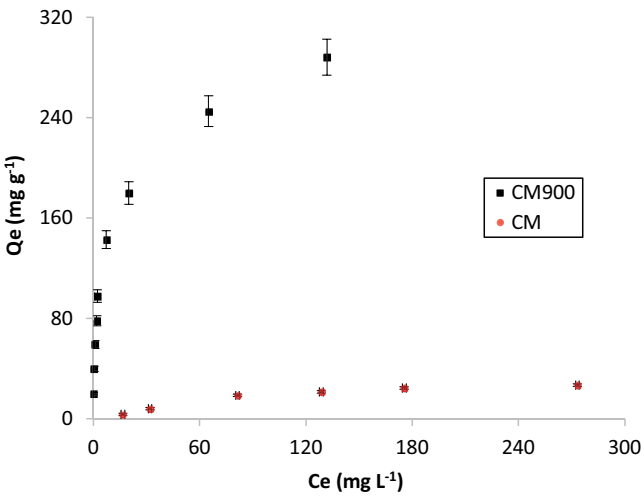

Fig. 5. Adsorption affinity of Congo red by carbonate material and CM900 at 40°C.

The Langmuir model led to a significant divergence between experimental and theoretical values of the amount adsorbed at equilibrium, up to 47% for CM at 25°C and 42% for CM900 at 40°C, which shows the inadequacy of this model. Among the assumptions of the Langmuir model are that the adsorption sites are both similar and energetically equivalent, which seems unlikely for our carbonate materials. The Freundlich model is also unsuitable for our data for the same reasons as the Langmuir model. An important limitation of the Freundlich model is that it does not describe a limit in adsorption capacity, while carbonate materials have a limited pore volume. The Redlich–Peterson model equation contains three parameters and is applicable for both heterogeneous and homogeneous adsorption. As shown in Table 5, this model gives a good description of CR adsorption by both CM and CM900. The coefficient of determination and relative error values are overall ≥0.97 and <10.0%,

Table 4
Comparison of uptake capacities of CR with other adsorbents

Adsorbents	Q_{max} (mg·g^{-1})	References
Sawdust	5.1	[39]
Activated carbon	32.9	[40]
Eichhonia charcoal	56.8	[41]
Modified halloysites (AH600-5N)	85.1	[42]
Penicillium glabrum	101.0	[43]
Bentonite	158.7	[15]
Calcium alginate	181.2	[16]
$Ni(OH)_2$	206.2	[44]
Carbonate material (CM)	32.7	This study
Carbonate material (CM900)	288.2	This study

Table 5
Isotherm parameters for the Congo red adsorption on carbonate materials CM and CM900

Parameters	Models	Adsorbents			
		CM		CM900	
		25°C	40°C	25°C	40°C
Langmuir	Q_{exp} (mg·g^{-1})	26.36	32.73	261.36	288.3
	Q_m (mg·g^{-1})	40.16	42.65	268.30	340.54
	K_L (L·mg^{-1})	0.0090	0.0032	0.1960	0.0150
	R^2	0.9841	0.9328	0.9601	0.9509
	E (%)	46.87	40.11	14.97	42.01
Freundlich	K_F (L·mg^{-1})$^{1/n}$	0.712	1.969	22.68	72.66
	n	0.520	0.463	0.430	0.281
	R^2	0.935	0.992	0.961	0.993
	E (%)	33.03	30.25	18.63	7.73
Redlich–Peterson	K_{RP} (L·g^{-1})	0.062	0.901	9.510	470.15
	β	1.524	0.927	0.713	0.722
	a_{RP} (L·mg^{-1})β	0.277	0.732	0.133	5.578
	R^2	0.972	0.988	0.981	0.996
	E (%)	8.02	10.85	7.16	8.42

respectively. The Redlich–Peterson model also successfully fitted CR adsorption isotherms by a modified halloysite [42]. The β exponent is overall lower than 1, which reflect a favorable adsorption on heterogeneous energy sites. The K_{RP} values of CM900 increase with increasing temperature and are significantly higher than those of CM. As they provide an indication on adsorption capacity, the resulting values are consistent with the equilibrium data obtained.

3.2.5. Thermodynamic parameters

Thermodynamic parameters are summarized in Table 6. Negative values of $\Delta G°$ show that the adsorption of CR is spontaneous. The spontaneous character of adsorption has been reported by several authors for different pollutant-material systems [45–47]. Spontaneity changes as follows: CM900 > CM, depending on the degree of adsorption. Regardless of the material, the $\Delta G°$ values decrease with increasing temperature from 298 to 328 K, suggesting that adsorption is more favorable at high temperatures. The positive values of $\Delta H°$ show that the removal of CR is endothermic. The positive value of the generated entropies ($\Delta S° > 0$) is a consequence of the loss of the structured water surrounding the solute molecules and the release of those of water from the surface of carbonate materials, due to the transfer of CR molecules from solution to the surface of carbonate materials [48]. The reduction in solvent organization and thus a sharp entropy increase in the system ($\Delta S° > 0$) is significant enough to cause a spontaneous reaction ($\Delta G° < 0$).

3.2.6. FTIR analysis after CR adsorption

FTIR spectroscopy technique was used to elucidate the adsorption mechanism. The infrared spectra of CM900 and CR, before and after adsorption (CR-loaded CM900), were recorded in the 4,000–400 cm^{-1} range (Fig. 6). The acute peak at 3,703 cm^{-1} (CM900) could be due to a hydroxyl (OH) associated with MgO as hydroxylated magnesium oxide [49]. The band at 562 cm^{-1} may be also related to MgOH species [50]. The characteristics of the CR bands were given in a previous paper [42]. After exposing CM900 to a 400 mg·L^{-1} solution of Congo red, the spectrum obtained (Fig. 6–Congo red-loaded CM900) reveals several changes: some bands disappear, while others move and change in intensity. These spectral features underline the interaction of Congo red with the chemical species available on the CM900 surface. The reduction in intensity of the 3,430; 1,578; 1,226 and 531 cm^{-1} bands denotes the implication of amine groups belonging to the Congo red.

Table 6
Thermodynamic parameters for the Congo red adsorption onto carbonate materials

Adsorbents	$\Delta H°$ (kJ·mol^{-1})	$\Delta S°$ (J·mol^{-1}·K^{-1})	$\Delta G°$ (kJ·mol^{-1})		
			298 K	313 K	328 K
CM	27.64	141.70	–14.58	–16.70	–18.83
CM900	123.71	474.91	–17.81	–24.93	–32.06

3.3. Desorption and regeneration

Desorption and regeneration provide valuable indications on the regeneration potential of our best adsorbent. Five eluents were employed to remove CR from CM900 (Fig. 7). Water is the least efficient eluent since 7% of CR was recovered at 40°C, which means that the CR molecules

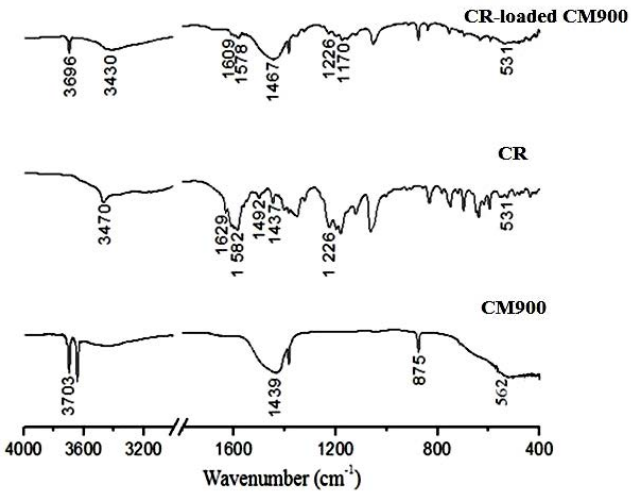

Fig. 6. Fourier-transform infrared spectra of CM900, Congo red (CR) and CR-loaded CM900.

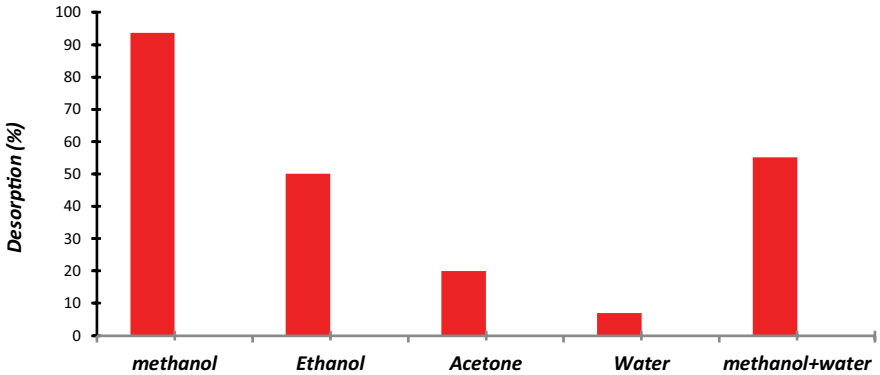

Fig. 7. Desorption rate of Congo red from CM900 with different solvents.

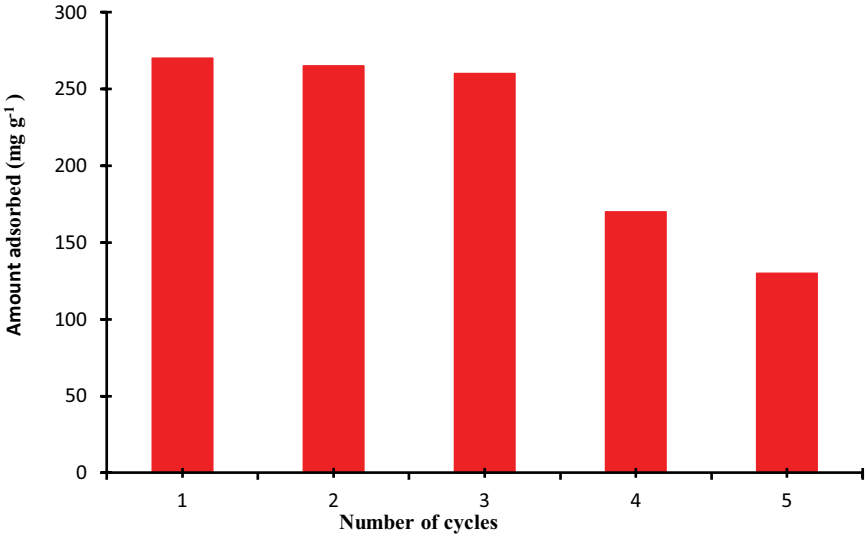

Fig. 8. Amount of Congo red adsorbed by CM900 according to successive cycles.

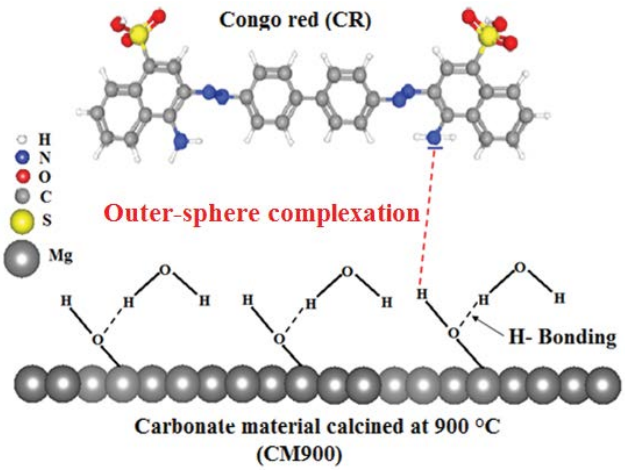

Fig. 9. Mechanism of the Congo red-CM900 interaction.

have a better affinity for CM900. Methanol has the highest desorption capacity with 94% of the total adsorbed amount. A 94% extraction rate would mean that CR physically interacts with CM900. CR is highly soluble in alcohols due to their organic and polar fractions. In addition, reducing the molecular weight of alcohols can improve their desorption performance, as small molecules easily penetrate the lattice of the carbonate material and extract CR. This would explain why the desorption capacity of methanol (MW = 32) is better than that of ethanol (MW = 46).

Regeneration ease is an important factor in the industry applications of any adsorbent. Five adsorption/desorption cycles were tested with methanol as solvent (Fig. 8). CM900 conserves a comparable adsorption capacity for three cycles. It subsequently decreases for the fourth and fifth cycles. Among the problems experienced, an amount of CM900 was lost at each adsorption–desorption stage. A further difficulty is that at each desorption, methanol permanently occupied the adsorption sites [51].

3.4. Interaction mechanism

From FTIR analysis, it is evident that the CR-CM900 interaction occurs between amine groups of Congo red and MgOH species available on the CM900 surface. This interaction is physical in nature based on the parameters explored. Ikhsan et al. [52] showed that an outer-sphere complexation occurs between aminopyridinium groups and montmorillonite, while Yan et al. [53] showed that MgOH acts as an adsorbent by involving outer-sphere complexation. Therefore, it is reasonable to assume that the amine groups of Congo red would interact with the MgOH species of CM900 through outer-sphere complexation. Such an interaction is physical in nature in accordance with the discussion given in this paper. On this basis, we represented the interaction of CR with CM900 in Fig. 9.

4. Conclusion

A carbonate material was treated at 900°C and characterized by XRD and SEM analyses. The characterization results explained the adsorption capacity of CM900 and CM with respect to Congo red, an anionic azo dye. A full decarbonation in CaO and MgO, at 900°C, and a more porous structure justified why CM900 adsorbs significantly more CR than CM, that is, 288.2 and 32.7 mg·g^{-1}, respectively. The pseudo-first-order model adequately described the kinetic data. The experimental isotherms were suitably fitted by the Redlich–Peterson model. Thermodynamic parameters suggested a spontaneous and endothermic process. Methanol easily desorbed the CR adsorbed by CM900 which maintained its adsorption capacity during three adsorption–desorption cycles. The mechanistic study highlighted an outer-sphere complexation between the amine groups of CR and the MgOH species of CM900.

References

[1] N. Abbasi, S.A. Khan, T.A. Khan, Response surface methodology mediated process optimization of Celestine

blue B uptake by novel custard apple seeds activated carbon/ $FeMoO_4$ nanocomposite, J. Water Process Eng., 41 (2021) 102267, doi: 10.1016/j.jwpe.2021.102267.
[2] T.A. Khan, A.A. Mukhlif, E.A. Khan, Uptake of Cu^{2+} and Zn^{2+} from simulated wastewater using muskmelon peel biochar: isotherm and kinetic studies, Egypt. J. Basic Appl. Sci., 4 (2017) 236–248.
[3] T.A. Khan, M. Nazir, E.A. Khan, Magnetically modified multiwalled carbon nanotubes for the adsorption of Bismarck brown R and Cd(II) from aqueous solution: batch and column studies, Desal. Water Treat., 57 (2016) 19374–19390.
[4] T.A. Khan, R. Rahman, E.A. Khan, Decolorization of Bismarck brown R and crystal violet in liquid phase using modified pea peels: non-linear isotherm and kinetics modeling, Model. Earth Syst. Environ., 2 (2016) 1–11.
[5] G. Crini, Non-conventional low-cost adsorbents for dye removal: a review, Bioresour. Technol., 97 (2006) 1061–1085.
[6] Y.O. Khaniabadi, M. Javad Mohammadi, M. Shegerd, S. Sadeghi, S. Saeedi, H. Basiri, Removal of Congo red dye from aqueous solutions by a low-cost adsorbent: activated carbon prepared from *Aloe vera* leaves shell, Environ. Health Eng. Manage. J., 4 (2017) 29–35.
[7] O. Bashir, M.N. Khan, T.A. Khan, Z. Khan, S.A. AL-Thabaiti, Influence of stabilizing agents on the microstructure of Co-nanoparticles for removal of Congo red, Environ. Technol. Innovation, 7 (*2017*) 1965–1977.
[8] D. Cui, Y.Q. Guo, H.S. Lee, H.Y. Cheng, B. Liang, F.Y. Kong, Y.Z. Wang, L.P. Huang, M.Y. Xu, A.J. Wang, Efficient azo dye removal in bioelectrochemical system and post-aerobic bioreactor: optimization and characterization, Chem. Eng. J., 243 (2014) 355–363.
[9] G. Han, Y. Du, Y. Huang, W. Wang, S. Su, B. Liu, Study on the removal of hazardous Congo red from aqueous solutions by chelation flocculation and precipitation flotation process, Chemosphere, 289 (2022) 133109, doi: 10.1016/j.chemosphere.2021.133109.
[10] A. Nora'aini, A. Norhidayah, A. Jusoh, The role of reaction time in organic phase on the Preparation of thin-film composite nanofiltration (TFC-NF) membrane for dye removal, Desal. Water Treat., 10 (2009) 181-191.
[11] F. Bessaha, N. Mahrez, S. Bendenia, F. Kasmi, K. Marouf-Khelifa, A. Khelifa, Characterization and spectroscopic study of a heat-treated and acid-leached halloysite used in Congo red adsorption, Int. J. Intell. Eng. Syst., 10 (2017) 272–279.
[12] D. Hussain, S.A. Khan, S.S. Alharthi, T.A. Khan, Insight into the performance of novel kaolinite-cellulose/cobalt oxide nanocomposite as green adsorbent for liquid phase abatement of heavy metal ions: modelling and mechanism, Arabian J. Chem., 15 (2022) 103925, doi: 10.1016/j.arabjc.2022.103925.
[13] A. Aljeboree, A. Alshirifi, A. Alkaim, Kinetics and equilibrium study for the adsorption of textile dyes on coconut shell activated carbon, Arabian J. Chem., 10 (2017) S3381-S3393.
[14] T.A. Khan, S. Sharma, E.A. Khan, A.A. Mukhlif, Removal of Congo red and basic violet 1 by chir pine (*Pinus roxburghii*) sawdust, a saw mill waste: batch and column studies, Toxicol. Environ. Chem., 96 (2014) 555–568.
[15] E. Bulut, M. Ozacar, I.A. Sengil, Equilibrium and kinetic data and process design for adsorption of Congo red onto bentonite, J. Hazard. Mater., 154 (2008) 613–622.
[16] V.S.M. Dong-Su Kim, Equilibrium isotherms, kinetics, and thermodynamics studies for Congo red adsorption using calcium alginate beads impregnated with nano-goethite, Ecotoxicol. Environ. Saf., 141 (2017) 226–234.
[17] A. Zahir, Z. Aslam, MS. Kamal, W. Ahmad, A. Abbas, R. Shawabkeh, Development of novel cross-linked chitosan for the removal of anionic Congo red dye, J. Mol. Liq., 244 (2017) 211–218.
[18] A. Lavat, M. Grasselli, Synthesis and characterization of ceramic materials based on the system MgO-CaO-TiO_2 from dolomite, Procedia Mater. Sci., 8 (2015) 162–171.
[19] C. Sadik, O. Moudden, A. El Bouari, I.-E. El Amrani, Review on the elaboration and characterization of ceramics refractories based on magnesite and dolomite, J. Asian Ceram. Soc., 4 (2016) 219–233.
[20] I. Belarbi, A. Çoruh, R. Hamacha, K. Marouf-Khelifa, A. Khelifa, Development and characterization of a new dolomite-based catalyst: application to the photocatalytic degradation of pentachlorophenol, Water Sci. Technol., 79 ((2019) 741–752.
[21] B. Valle, N. García-Gómez, A. Remiro, A.G. Gayubo, J. Bilbao, Cost-effective upgrading of biomass pyrolysis oil using activated dolomite as a basic catalyst, Fuel Process. Technol., 195 (2019) 106142, doi: 10.1016/j.fuproc.2019.106142.
[22] F. Boucif, K. Marouf-Khelifa, I. Batonneau-Gener, J. Schott, A. Khelifa, Preparation, characterization of thermally treated Algerian dolomite powders and application to azo-dye adsorption, Powder Technol., 201 (2010) 277–282.
[23] S. Lagergren, Zur theorie der sogenannten adsorption geloster stoffe, Zur theorie der sogenannten adsorption geloster stoffe, Kungliga SvenskaVetenskapsademiens, Handlingar, 24 (1898) 1–39.
[24] Y.S. Ho, G. McKay, Pseudo-second-order model for sorption process, Process Biochem. (Oxford, U.K.), 34 (1999) 451–465.
[25] W.J. Weber, J.C. Morris, Kinetics of adsorption of carbon from solution, J. Sanit. Div. Am. Soc. Civ. Eng., 89 (1963) 31–59.
[26] S.H. Chien, W.R. Clayton, Application of Elovich equation to the kinetics of phosphate release and sorption in soils, Soil Sci. Soc. Am. J., 44 (1980) 265–268.
[27] I. Langmuir, Adsorption of gases on plane surfaces of glass, mica and platinum, J. Am. Chem. Soc., 40 (1918) 1361–1403.
[28] H.M.F. Freundlich, Over the adsorption in solution, J. Phys. Chem., 57 (1906) 385–471.
[29] O. Redlich, D.L. Peterson, A useful adsorption isotherm, J. Phys. Chem., 63 (1959) 1024-1033.
[30] A.H. de Aza, M.A. Rodriguez, J.L. Rodriguez, S. de Aza, P. Pena, P. Convert, T. Hansen, X. Turrillas, Decomposition of dolomite monitored by neutron thermodiffractometry, J. Am. Ceram. Soc., 8 (2002) 881–888.
[31] M. Khelifa, S. Mellouk, G.L. Lecomte-Nana, I. Batonneau-Gener, K. Marouf-Khelifa, A. Khelifa, Methodological approach to the chloramphenicol adsorption by acid-leached halloysites: preparation, characterization, performance and mechanism, Microporous Mesoporous Mater., 348 (2023) 112412, doi: 10.1016/j.micromeso.2022.112412.
[32] S. Ziane, K. Marouf-Khelifa, H. Benmekki, J. Schott, A. Khelifa, Removal of a reactive textile azo dye by dolomitic solids: kinetic, equilibrium, thermodynamic, and FTIR studies, Desal. Water Treat., 56 (2015) 695–708.
[33] N.E.H. Larbi, D.R. Merouani, H. Aguedal, A. Iddou, A. Khelifa, Removal of heavy metals Cd(II) and Al(III) from aqueous solutions by an eco-friendly biosorbent, Key Eng. Mater., 800 (2019) 181–186.
[34] F. Tang, D. Gao, L. Wang, Y. He, P. Song, R. Wang, Preparation of grafting copolymer of acrylic acid onto loess surface and its adsorption behavior, Water Sci. Technol., 82 (2020) 673–682.
[35] A. Saeed, M. Sharif, M. Iqbal, Application potential of grapefruit peel as dye sorbent: kinetics, equilibrium and mechanism of crystal violet adsorption, J. Hazard. Mater., 179 (2010) 564–572.
[36] A. Khalfa, S. Mellouk, K. Marouf-Khelifa, A. Khelifa, Removal of catechol from water by modified dolomite: performance, spectroscopy, and mechanism, Water Sci. Technol., 77 (2018) 1920–1930.
[37] F. Salaa, S. Bendenia, G.L. Lecomte-Nana, A. Khelifa, Enhanced removal of diclofenac by an organohalloysite intercalated via a novel route: performance and mechanism, Chem. Eng. J., 396 (2020) 125226, doi: 10.1016/j.cej.2020.125226.
[38] F. Boucif, D.R. Merouani, K. Marouf-Khelifa, A. Khelifa, Adsorption of Orange I by modified dolomite: performance and mechanism, Int. J. Environ. Sci. Technol., 18 (2021) 3179–3188.
[39] V.S. Mane, P.V. Vijay Babu, Kinetic and equilibrium studies on the removal of Congo red from aqueous solution using Eucalyptus wood (*Eucalyptus globulus*) saw dust, J. Taiwan Inst. Chem. Eng., 44 (2013) 81–88.
[40] M. Abbas, M. Trari, Kinetic, equilibrium and thermodynamic study on the removal of Congo red from aqueous solutions

by adsorption onto apricot stone, Process Saf. Environ. Prot., 98 (2015) 424–436.
[41] K. Sumanjit, R.Seema, M. Rakesh Kumar, Adsorption kinetics for the removal of hazardous dye Congo red biowaste materials as adsorbents, J. Chem., 2013 (2013) 628582, doi: 10.1155/2013/628582.
[42] F. Bessaha, N. Mahrez, K. Marouf-Khelifa, A. Çoruh, A. Khelifa, Removal of Congo red by thermally and chemically modified halloysite: equilibrium, FTR spectroscopy, and mechanism studies, Int. J. Environ. Sci. Technol., 16 (2019) 4253–4260.
[43] H.D. Bouras, A.R. Yeddou, N. Bouras, D. Hellel, M.D. Holtz, N. Sabaou, A. Chergui, B. Nadjem, Biosorption of Congo red dye by *Aspergillus carbonarius* M333 and *Penicillium glabrum* Pg1: kinetics, equilibrium and thermodynamic studies, J. Taiwan Inst. Chem. Eng., 80 (2017) 915–923.
[44] M. Yang, Y. Wu, R. Rao, H. Wang, Methanol promoted synthesis of porous hierarchical α-$Ni(OH)_2$ for the removal of Congo red, Powder Technol., 320 (2017) 377–385.
[45] D. Hussain, S.A. Khan, T.A. Khan, Fabrication and characterization of mesoporous guar gum/$NiWO_4$ nanocomposite for efficient adsorption of Phloxine B and Crystal violet from aqueous solution and evaluation of its antioxidant activity, Colloid Interface Sci. Commun., 44 (2021) 100488, doi: 10.1016/j.colcom.2021.100488.
[46] M.F. Siddiqui, S.A. Khan, D. Hussain, U. Tabrez, I. Ahamad, T. Fatma, T.A. Khan, A sugarcane bagasse carbon-based composite material to decolor and reduce bacterial loads in wastewater from textile industry, Ind. Crops Prod., 176 (2022) 114301, doi: 10.1016/j.indcrop.2021.114301.
[47] N. Abbasi, S.A. Khan, T.A. Khan, S.S. Alharthi, Statistical evaluation of liquid phase sequestration of acridine orange and Cr^{6+} by novel mesoporous glutamic acid-g-polyacrylamide/plaster of paris/riboflavin hydrogel nanocomposite, Environ. Res., 213 (2022) 113712, doi: 10.1016/j.envres.2022.113712.
[48] V.O. Leone, M.C. Pereira, S.F. Aquino, L.C.A. Oliveira, S. Correa, T.C. Ramalho, L.V.A. Gurgel, A.C. Silva, Adsorption of diclofenac on a magnetic adsorbent based on maghemite: experimental and theoretical studies, New J. Chem., 42 (2018) 437–449.
[49] J. Ji, Y. Ge, W. Balsam, J.E. Damuth, J. Chen, Rapid identification of dolomite using a Fourier transform infrared spectrophotometer (FTIR): a fast method for identifying Heinrich events in IODP Site U1308, Mar. Geol., 258 (2009) 60–68.
[50] E.F. de Oliveira, Y. Hase, Infrared study of magnesium–nickel hydroxide solid solutions, Vib. Spectrosc., 31 (2003) 19–24.
[51] J. Chern, C. Wu, Desorption of dye from activated carbon beds: effects of temperature, pH, and alcohol, Water Res., 35 (2001) 4159–4165.
[52] J. Ikhsan, M.J. Angove, J.D. Wells, B.B. Johnson, Surface complexation modeling of the sorption of 2-, 3-, and 4-aminopyridine by montmorillonite, J. Colloid Interface Sci., 284 (2005) 383–392.
[53] H. Yan, J. Bai, X. Chen, J. Wang, H. Zhang, Q. Liu, M. Zhang, L. Liu, High U(VI) adsorption capacity by mesoporous $Mg(OH)_2$ deriving from MgO hydrolysis, RSC Adv., 3 (2013) 23278–23289.